

# Continuous and Reversible Electrical Tuning of Fluorescent Decay Rate via Fano Resonance

Emre Ozan Polat<sup>(1,2,6,+)</sup>,\* Zafer Artvin<sup>(3,6)</sup>, Yusuf Şaki<sup>(3,6)</sup>, Alpan Bek<sup>(3,6)</sup>, and Ramazan Sahin<sup>(4,5,6,+)</sup>†

(1) Department of Physics, Bilkent University, 06800 Ankara, Turkey

(2) UNAM- National Nanotechnology Research Center and Institute of Materials Science and Nanotechnology, Bilkent University, 06800 Ankara, Turkey

(3) Department of Physics, Middle East Technical University, 06800 Ankara, Turkey

(4) Department of Physics, Akdeniz University, 07058 Antalya, Turkey

(5) Türkiye National Observatories, TUG, 07058, Antalya, Türkiye

(6) Institute of Nuclear Sciences, Hacettepe University, 06800 Ankara, Turkey and

(+) These two authors contributed equally to this work.

(Dated: December 31, 2024)

Decay rate of an atomic or molecular dipole depends on the local density of optical states (LDOS) —Purcell effect— which can significantly be enhanced near a dielectric-core metal-shell nanoparticle (CSNP). On top of that, an auxiliary quantum object (QO) can introduce a Fano transparency in the plasmonic spectrum of the CSNP. Here, we show that an auxiliary QO, located at the hotspot of the CSNP, can modify the LDOS, hence the decay rate of an excited dipole. Moreover, by controlling the resonance of the auxiliary QO via an applied voltage, one can continuously and reversibly tune both the radiative and nonradiative decay rates of the dipole up to 2 orders-of-magnitude. This phenomenon emerges as an invaluable tool to implement in integrated quantum technologies, enabling realization of on-demand entanglement/single-photon sources, controlled execution of quantum gates and electrical-control of superradiant-like phase transitions. It also bears potential for application in super-resolution microscopy and surface-enhanced Raman spectroscopy (SERS).

## I. Introduction

Electromagnetic interaction between an atomic system and a closely located metal nanostructure (MNS) has provided a viable platform for researchers to investigate the nature of nanophotonic phenomena yielding series of notable innovations such as SERS, that allows for single molecule detection [1], single photon transistors realizing strong nonlinear interactions at the single-photon level [2], and cavity-free subwavelength confinement of optical fields using 0D-1D structures [3]. At the heart of the demonstrated innovations lies the Purcell effect [4] which defines the change in the lifetime of an atomic/molecular excited state. It takes place due to the modifications in the number of available optical states (local density of optical states, LDOS) emitter can couple.

This, in turn, results in the enhancement or suppression of the spontaneous emission rate of the emitter. The effect is prominent especially when the molecular system is located in a resonant cavity [5] or near a MNS [6] that modifies the electromagnetic environment. The modified decay rate is given by the change in the LDOS with respect to free space, such as  $\gamma = (LDOS)_{\text{env}} / (LDOS)_{\text{free}} \times \gamma_0$  where  $\gamma_0$  is the free space decay rate. In the presence of an absorptive material, such as an MNS, enhanced molecular decay rate can take place both as photon emission and nonradiative photon transfer (absorption) into the MNS —apart from the intrinsic nonradiative losses within the emitter. The former demonstrates itself as

fluorescence enhancement [7] while the latter is linked to optical losses.

Active control of Purcell effect is a key to enable switchable light emitting nanophotonic devices which represents a fast-growing field due to its direct contribution to telecommunication and integrated quantum technologies [8–10]. While there exist studies on the control of spontaneous emission via Purcell effect, they mostly rely on altering the cavity size/parameters representing a passive control scheme [11–13]. Cavity-dependent demonstrations of Purcell effect have attracted great attention due to the ability to tune the fluorescence emission spectra of molecules. However, it comes with certain limitations for active control of Purcell effect such as fixed cavity components and mirror spacings [14]. Although this limitation was partially solved within a tunable microcavity scheme, the applicability of the approach is still limited in the context of integrated circuits due to the requirement of immersion oils and CMOS incompatible elements [15].

Alternatively, some active methods to switch photoluminescence (PL) have also been demonstrated using various physical phenomena such as quantum confined stark effect [16, 17], electric field induced quenching [18], Förster resonant energy transfer (FRET) [19], and implementation of electroactive polymers in redox reaction [20, 21]. Although it was shown to be possible to switch fluorescence actively, these methods utilize quenching in order to turn off the fluorescence. That is, molecular excitation is almost completely transferred (lost) into the MNS and not kept in the emitter. Moreover, the modulation depths are poor and some of the studies report only a limited number of successive modulations due to hys-

\* emre.polat@bilkent.edu.tr

† rsahin@itu.edu.tr

teresis in the cyclic performance prohibiting a complete recovery between on and off states [19–21]. Furthermore, the response time of those applications reaches maximum millisecond regime which is not compatible with CPU clock speed range (GHz) and barely supports current display technology with frame rates (FPS) of 60-144 Hz. Despite the attempts to use reverse bias providing 200:1 contrast ratio and 300 ns response time [22], the usage of extremely high ( $3 \times 10^6$  V/cm<sup>2</sup>) external field prohibits the technological use of reported methodologies.

Therefore, achieving continuous and reversible control within a compact device geometry that provides large modulation depths with (and over) CPU clock speed compatibility remains as a great challenge in active control of fluorescence for technology applications.

In this paper, we provide a proof-of-principle demonstration of active and reversible tuning of both radiative and nonradiative decay rates of a fluorescent molecule (FM). We electrically tune the LDOS by shifting the position of a Fano transparency (also known as Fano resonance) [23–25]. The resonance of the Fano transparency, induced by a quantum object (QO) residing at the CSNP hotspot (Fig. 1a), is tuned by shifting the level-spacing of the QO via an applied voltage. This way, the decay rates can be continuously tuned between  $\gamma=1-215\gamma_0$  within a “picosecond” response time which is limited by the read-out rate of the circuit operation (GB/s). We emphasize that the demonstrated system is fundamentally different from previously reported active PL switching and modulation effects that are based on screening of the PL for an external observer. By trapping the fluorescent state in the molecule (i.e., not quenching it), the nature of our switching process exhibits a crucial property with the ability to hold and release the interested fluorescent state by voltage application.

In our demonstrated system, the presence of a plasmonic SiO<sub>2</sub>/Ag core (SiO<sub>2</sub>) shell (Ag) nanoparticle (CSNP) boosts the LDOS of a FM (Fig. 1a). When an auxiliary QO, such as a quantum dot (QD) or a defect-center of resonance  $\omega_{QO}$  is positioned near the CSNP, it introduces a Fano transparency at  $\omega_{QO} = \omega_{FM}$  [26]. Fano transparency is the plasmon-analog of electromagnetically-induced-transparency (EIT) [27]. Coupling of a dark mode or a QO to a bright plasmon mode introduces two paths for the absorption [28]. When the two paths work out of phase, absorption is canceled, and a transparency window appears in the spectrum of the MNS [29]. Therefore, an absorption and scattering dip appears at  $\omega_{QO}$ . In this work, by choosing  $\omega_{QO}$  about the transition frequency  $\omega_{FM}$  of the FM’s metastable (fluorescence) state (Fig. 1b), we show that the presence of the QO turns off the LDOS that used to be enhanced due to the presence of the CSNP (Fig. 2a). In other words, at  $\omega_{QO} = \omega_{FM}$  turns off the extra LDOS occurring due to the presence of the CSNP. Additionally, it also turns off the nonradiative decay rate emerging due to the dissipation at the Ag shell (Fig. 2b).

More interestingly, as the QO’s resonance can be

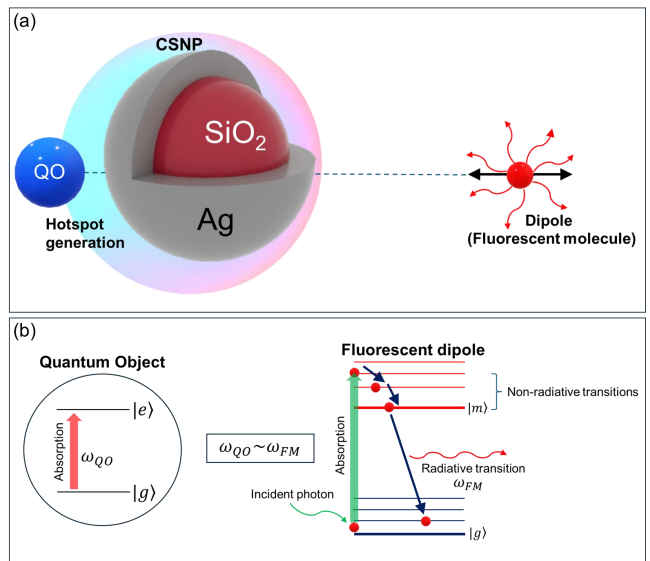


FIG. 1. Proof-of-principle illustration of the phenomenon on a sample configuration. (a) An auxiliary QO, representing a dense collection of defect-centers or densely ion-planted G-centers is positioned at the hotspot. FM (dipole) whose decay rates are of interest is located at 15 nm distance. (b) The two-level QO and the Jablonski diagram of the FM. The absorption frequency of the QO ( $\omega_{QO}$ ) and radiative transition of the dipole ( $\omega_{FM}$ ) are similar. The QO introduces a Fano transparency in the spectrum of the CSNP that controls the CSNP-induced LDOS.

shifted [30, 31] via applied voltage (Fig. 3a), the decay rate patterns of Figs. 2a and 2b are also shifted electrically, enabling the continuous tuning of the decay rates (Figs. 3b and 3c). Thus, the LDOS, which is initially enhanced due to the CSNP, can also be tuned continuously via the applied voltage within sub-picosecond response time. We emphasize that a 20 meV resonance shift can tune the radiative decay rate between  $\gamma_r=1-215\gamma_0$  continuously.

This method, being reversible and cavity-free, allows for nanofabrication approaches for the integration in quantum circuits and conventional Si-based readout circuits (see the Supplementary Material, SM). Compared to active electroluminescent counterparts, Fano resonance provides an incomparably large range of tuning corresponding to 215 times (21500%) modulation. It presents technologically compatible operation frequencies since the response time of the Fano resonance is of the order of picosecond and therefore the tuning rate is only limited by the speed of the solid-state device. We believe that the demonstrated method manifests itself as an invaluable tool that enables so-far unrealized implementations ranging from voltage-controlled superpositions of hyperfine states to on-demand single-photon imaging techniques.

## II. Results

Fig. 1a shows a sample configuration we have simulated as a proof-of-principle demonstration of the phenomenon. In our simulations we use a  $\text{SiO}_2/\text{Ag}$  CSNP of diameter 105 nm where plasmonic losses limiting the use of MNSs in optoelectronics are compensated via optical gain incorporated in the core insulator ( $\text{SiO}_2$ ) region (100 nm in diameter) [32, 33]. The Ag-shell is a 5 nm thick layer that is deposited uniformly on the  $\text{SiO}_2$  core. An auxiliary QO of 40 nm diameter representing a densely implanted G-centers (or nitrogen-vacancy (NV) defect centers) [34–36] is located 5 nm to the Ag-shell and introduces the Fano transparency at  $\omega_{\text{QO}}$ . FM (dipole), polarized along the x-axis, is positioned on the opposite side at 15 nm distance. We calculated the LDOS for the radiative and nonradiative decay rates of the dipole (fluorescent molecule FM) using finite difference time domain method (FDTD) [37]. In the demonstrated configuration, we first show that Fano transparency can switch off the initially enhanced emission (radiative decay) rate of the FM. Fig. 2a shows the radiative decay spectrum of the dipole (FM) with and without the QO in the system. The QO residing at the hotspot of the CSNP turns off the CSPN induced enhancement in the LDOS. Decay rate drops from  $215\gamma_0$  to  $\gamma_0$  at  $\omega_{\text{QO}} = \omega_{\text{FM}}$ . For other fluorescence wavelengths, decay rate suppression is weaker. One should note that decay of a molecule from its excited state always includes a quantum probabilistic nature [38]. The  $\gamma_0$  is to be understood as an expectation value.

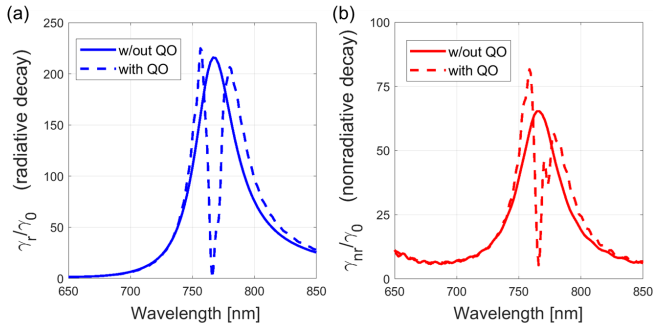


FIG. 2. Suppression of the (a) radiative ( $\gamma_r$ ) and (b) nonradiative ( $\gamma_{nr}$ ) decay rates by Fano resonance. A QO residing at the hotspot can turn off the CSNP-induced LDOS.

In Fig. 2b, we observe a similar effect for the nonradiative decay rate. The presence of the QO also suppresses the absorption losses that the CSNP induces initially. The nonradiative decay is suppressed down to  $5\gamma_0$  from  $65\gamma_0$ . We model the QO by a Lorentzian dielectric function [26, 28, 39] of resonance  $\omega_{\text{QO}}=766$  nm, linewidth  $\sim 10^{10}$  Hz and oscillator strength  $f = 0.2$ . We used the corresponding experimental dielectric functions for CSNP composed of Ag shell and  $\text{SiO}_2$  core materials [40, 41]. To show the promises of our method, we further study the voltage-controlled continuous tuning of the decay rates. Application of an external electric field on the

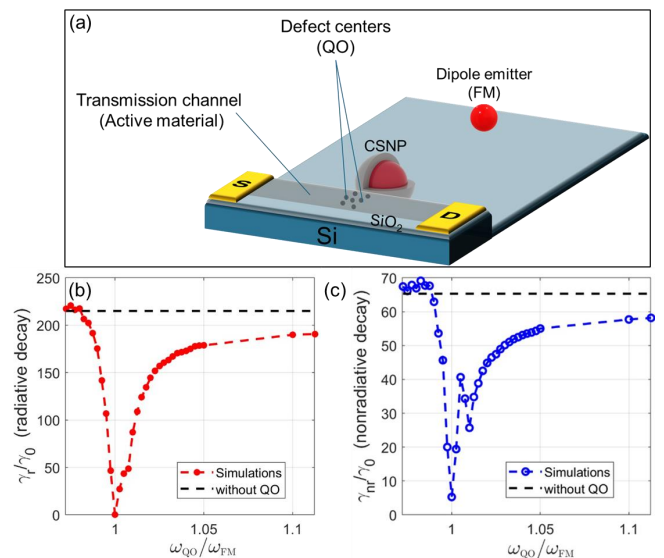


FIG. 3. Continuous electrical tuning of radiative and nonradiative decay rates. (a) Illustration of a possible device scheme for continuous electrical tuning of the decay rate. In a FET structure, the collection of defect centers [34, 35] that act as the modeled QO, are biased through source and drain electrodes and gated by Si substrate through the  $\text{SiO}_2$  dielectric. The step-like structure is used to align the center of CSNP to the defect centers. (b) Radiative decay rate of the fluorescent dipole molecule under the influence of electrically controlled Fano transparency. Shift of  $\omega_{\text{QO}}$  with respect to  $\omega_{\text{FM}}$  changes the efficiency of the suppression for each voltage step, allowing continuous electrical tuning of the decay rate. Only a  $\sim 20$  meV resonance tuning is enough to achieve the continuous control between  $\gamma_r=1-215\gamma_0$ . (c) A similar control over nonradiative decay rate is also possible.

QO shifts the resonance  $\omega_{\text{QO}}$  (Fig. 3a).

Thus, the dashed curves in Figs. 2a and 2b, in particular the dips, also shift. The FDTD simulations show that the radiative and nonradiative decay rates can be tuned between  $\gamma_r=1-215\gamma_0$  and  $\gamma_{nr}=5-70\gamma_0$ , respectively, in our sample setup (Figs. 3b and 3c). Moreover, as the electrical shift in the resonance is reversible, modulation of  $\gamma_r$  and  $\gamma_{nr}$  are also reversible. In Figs. 3b and 3c, the fluorescence is fixed at  $\omega_{\text{FM}} = 766$  nm and  $\omega_{\text{QO}}$  is altered. Only a  $\sim 20$  meV tuning of the QO resonance is sufficient for such a control noting that much larger shifts have already been reported even for 1V of applied potential [42].

Fig. 3a shows the schematic illustration of a possible device where the collection of the defect centers is modelled as the QO. Several experimental methods have been reported for the formation of G-centers in  $\text{Si}/\text{SiO}_2$  as well as NV centers in diamond, such as the incorporation of carbon rich Si crystals in reactive ion etching process [35], functionalization of Si surface with organic molecules [34] and hot ion implementation in diamond [36]. In our model, by representing a collection of G-centers as a QO, the external field is provided through the

gate of a field-effect transistor (FET), where the active material that contains defect centers are biased through the source-drain channel. To provide the agreement between our model and the FET scheme, a step-like structure is employed merely to provide the spatial alignment of the defect centers to the CSNP. We note that an inhomogeneous broadening among the resonances of, e.g., G-centers results a similar broadening in the Fano transparency dip in Figs. 2a and 2b. In this case, even better control over relatively broader fluorescence spectra can be achieved.

Thus, we numerically demonstrate that we can actively control both the radiative and nonradiative decay rates of a FM for a narrow wavelength regime in a cavity-free environment. Our simulations were originally performed in vacuum therefore the dielectric environment of any possible device scheme (as shown in Figure 3a) would shift the plasmon resonances. This, however, won't change the nature of the demonstrated phenomenon.

### III. Conclusion, Discussion and Outlook

We provide a proof-of-principle numerical demonstration for the voltage-tunability of decay rates. Our simulations —exact solutions of Maxwell equations— show 2-orders magnitude modulation in the decay rate. A QO turns off the CSNP induced LDOS at fluorescence  $\omega_{\text{QO}} = \omega_{\text{FM}}$ . When  $\omega_{\text{QO}}$  is shifted by an applied voltage (Fig. 3a), the schemes (Figs. 2a and 2b) for the decay rates also shift, enabling a continuous tuning of these rates in Figs. 3b and 3c.

The phenomenon addresses a wide range of applications as we are demonstrating a fundamental issue in light-matter interaction, that is electrical-tuning of LDOS. This provides an invaluable tool especially for integrated quantum technologies. The technique offers ultimate control over on-demand single-photon sources and entanglement generation in circuits. These also imply voltage-controlled quantum gate operations. The phenomenon of superradiant phase transition, which depends on the decay rate, now can be electrically turned on/off in an integrated circuit. Thus, normal and super-radiant phase transitions between zero and a very strong entanglement state [43], can be employed to serve as a controllable collective entanglement resource in the integrated circuits. In addition, quantum batteries can become voltage-controlled based on the demonstrated phenomenon [44, 45].

Change in the LDOS not only alters the decay rates but can also tune coupling of a fixed intensity light to dipoles. This enables electrical tuning of light-matter interaction and stimulated transitions in ion-trap configurations. It is worth noting that the coefficients among two or more hyperfine states can be tuned very quickly without neces-

sitating a change in the pump intensity of different polarizations [46]. For appropriate choice of MNS-shapes (i.e. helical MNSs with spin angular momentum), the phenomenon can be used to enhance/control LDOS selectively among different polarizations. Thus, the method provides a compact, voltage-tunable and fast preparation of single atom/ion states or collective states of their ensembles. For direct applications with the state-of-the-art ion traps, however, one also needs to take extra care of interaction of MNS with the trap potentials, though such potentials result only weak couplings with MNSs. The same features are also valid for the quantum gate operations.

In this work, we study proof-of-principle demonstration of the phenomenon in free space where the tuning starts at  $\gamma_0$  and ranges to  $215\gamma_0$ . It is well studied that decay rates of FMs can be lowered down to values  $\gamma'_0$  that are much smaller than  $\gamma_0$ , e.g., when they are in photonic crystal cavities [47]. Such setups, in principle, can provide electrical tuning of decay rates in terms of the multiples of much smaller base values  $\gamma'_0$ . Demonstrated device structure can be achieved by various fabrication techniques and device construction schemes. (See the SM for details of reported fabrication steps.) Finally, the effect that we observe can be made more efficient by implementing more optimal setups.

We anticipate that the demonstrated technique can also be utilized in quantum optics for the on-demand generation of single-photons (or photon-pairs) and their synchronization with external systems such as a vibrating scanning probe microscopy (SPM) tip, or a confocal scanning laser microscope. Thanks to the ultimate control on the time gated activation of the emitter, the technique can also prove to be useful in performing spin-echo based quantum measurements/sensing applications such as quantum magnetometers [48] or quantum information processing [49]. Alternately, it can also serve as a voltage tunable band rejection filter for the radiative and nonradiative wavelengths falling into the corresponding Fano resonance linewidth. In general, the suitable execution of the demonstrated technique can form a base technology in the applications that require fine tuning of a specific fluorescence spectrum such as SERS and super-resolution microscopy.

### Acknowledgments

We gratefully thank Mehmet Emre Tasgin and Serkan Ates for discussions leading to this research. This research is conducted in the meetings that took place at Institute of Nuclear Sciences, Hacettepe University. E.O.P acknowledges the personal research fund (KAF) of Bilkent University. R.S. acknowledges support from TUBITAK No. 121F030 and 123F156.

---

[1] C. Serafinelli, A. Fantoni, E. C. Alegria, and M. Vieira, Plasmonic metal nanoparticles hybridized with 2D nano-

materials for SERS detection: A review, *Biosensors* **12**, 225 (2022).

- [2] D. E. Chang, A. S. Sørensen, E. A. Demler, and M. D. Lukin, A single-photon transistor using nanoscale surface plasmons, *Nature Physics* **3**, 807 (2007).
- [3] A. Akimov, A. Mukherjee, C. Yu, D. Chang, A. Zibrov, P. Hemmer, H. Park, and M. Lukin, Generation of single optical plasmons in metallic nanowires coupled to quantum dots, *Nature* **450**, 402 (2007).
- [4] E. M. Purcell, Spontaneous emission probabilities at radio frequencies, in *Confined Electrons and Photons: New Physics and Applications* (Springer, 1995) pp. 839–839.
- [5] K. J. Vahala, Optical microcavities, *Nature* **424**, 839 (2003).
- [6] J. R. Lakowicz, Radiative decay engineering 5: metal-enhanced fluorescence and plasmon emission, *Analytical Biochemistry* **337**, 171 (2005).
- [7] A. Camposeo, L. Persano, R. Manco, Y. Wang, P. Del Carro, C. Zhang, Z.-Y. Li, D. Pisignano, and Y. Xia, Metal-enhanced near-infrared fluorescence by micropatterned gold nanocages, *ACS Nano* **9**, 10047 (2015).
- [8] Y.-J. Lu, R. Sokhoyan, W.-H. Cheng, G. Kafaie Shirmanesh, A. R. Davoyan, R. A. Pala, K. Thyagarajan, and H. A. Atwater, Dynamically controlled purcell enhancement of visible spontaneous emission in a gated plasmonic heterostructure, *Nature Communications* **8**, 1631 (2017).
- [9] M. C. Munnix, A. Lochmann, D. Bimberg, and V. A. Haisler, Modeling highly efficient rcded-type quantum-dot-based single photon emitters, *IEEE Journal of Quantum Electronics* **45**, 1084 (2009).
- [10] D. Bimberg, E. Stock, A. Lochmann, A. Schliwa, J. A. Tofflinger, W. Unrau, M. Munnix, S. Rodt, V. A. Haisler, A. I. Toropov, *et al.*, Quantum dots for single-and entangled-photon emitters, *IEEE Photonics Journal* **1**, 58 (2009).
- [11] J. Canet-Ferrer, L. J. Martínez, I. Prieto, B. Alén, G. Muñoz-Matutano, D. Fuster, Y. González, M. L. Dotor, L. González, P. A. Postigo, *et al.*, Purcell effect in photonic crystal microcavities embedding InAs/InP quantum wires, *Optics Express* **20**, 7901 (2012).
- [12] A. Bennett, D. Unitt, P. See, A. Shields, P. Atkinson, K. Cooper, and D. Ritchie, Microcavity single-photon-emitting diode, *Applied Physics Letters* **86** (2005).
- [13] Y. Moritake, Y. Kanamori, and K. Hane, Emission wavelength tuning of fluorescence by fine structural control of optical metamaterials with fano resonance, *Scientific Reports* **6**, 33208 (2016).
- [14] M. Steiner, A. V. Failla, A. Hartschuh, F. Schleifenbaum, C. Stupperich, and A. J. Meixner, Controlling molecular broadband-emission by optical confinement, *New Journal of Physics* **10**, 123017 (2008).
- [15] A. Chizhik, F. Schleifenbaum, R. Gutbrod, A. Chizhik, D. Khoptyar, A. J. Meixner, and J. Enderlein, Tuning the fluorescence emission spectra of a single molecule with a variable optical subwavelength metal microcavity, *Physical Review Letters* **102**, 073002 (2009).
- [16] S. A. Empedocles and M. G. Bawendi, Quantum-confined stark effect in single cdse nanocrystallite quantum dots, *Science* **278**, 2114 (1997).
- [17] X. Xu, A. Andreev, and D. A. Williams, Manipulating quantum-confined stark shift in electroluminescence from quantum dots with side gates, *New Journal of Physics* **10**, 053036 (2008).
- [18] D. Bozyigit, O. Yarema, and V. Wood, Origins of low quantum efficiencies in quantum dot leds, *Advanced Functional Materials* **23**, 3024 (2013).
- [19] O. Salihoglu, N. Kakenov, O. Balci, S. Balci, and C. Kocabas, Graphene as a reversible and spectrally selective fluorescence quencher, *Scientific Reports* **6**, 33911 (2016).
- [20] R. Chen, Y. Gao, G. Zhang, R. Wu, L. Xiao, and S. Jia, Electric field induced fluorescence modulation of single molecules in pmma based on electron transfer, *International Journal of Molecular Sciences* **13**, 11130 (2012).
- [21] S. Wang, E. B. Berda, X. Lu, X. Li, C. Wang, and D. Chao, Tuning the fluorescent response of a novel electroactive polymer with multiple stimuli, *Macromolecular Rapid Communications* **34**, 1648 (2013).
- [22] S. Xie, H. Zhu, M. Li, and V. Bulović, Voltage-controlled reversible modulation of colloidal quantum dot thin film photoluminescence, *Applied Physics Letters* **120** (2022).
- [23] H. Leng, B. Szychowski, M.-C. Daniel, and M. Pelton, Strong coupling and induced transparency at room temperature with single quantum dots and gap plasmons, *Nature Communications* **9**, 4012 (2018).
- [24] M. F. Limonov, M. V. Rybin, A. N. Poddubny, and Y. S. Kivshar, Fano resonances in photonics, *Nature Photonics* **11**, 543 (2017).
- [25] M. E. Tasgin, A. Bek, and S. Postaci, Fano resonances in the linear and nonlinear plasmonic response, *Fano Resonances in Optics and Microwaves: Physics and Applications* **219** (2018).
- [26] X. Wu, S. K. Gray, and M. Pelton, Quantum-dot-induced transparency in a nanoscale plasmonic resonator, *Optics Express* **18**, 23633 (2010).
- [27] M. Fleischhauer, A. Imamoglu, and J. P. Marangos, Electromagnetically induced transparency: Optics in coherent media, *Reviews of Modern Physics* **77**, 633 (2005).
- [28] R. A. Shah, N. F. Scherer, M. Pelton, and S. K. Gray, Ultrafast reversal of a fano resonance in a plasmon-exciton system, *Physical Review B—Condensed Matter and Materials Physics* **88**, 075411 (2013).
- [29] C. L. Garrido Alzar, M. A. G. Martinez, and P. Nussenzeig, Classical analog of electromagnetically induced transparency, *American Journal of Physics* **70**, 37 (2002).
- [30] H. Larocque, M. A. Buyukkaya, C. Errando-Herranz, C. Papon, S. Harper, M. Tao, J. Carolan, C.-M. Lee, C. J. Richardson, G. L. Leake, *et al.*, Tunable quantum emitters on large-scale foundry silicon photonics, *Nature Communications* **15**, 5781 (2024).
- [31] D. A. Miller, D. Chemla, T. Damen, A. Gossard, W. Wiegmann, T. Wood, and C. Burrus, Electric field dependence of optical absorption near the band gap of quantum-well structures, *Physical Review B* **32**, 1043 (1985).
- [32] P. Rajput and M. S. Shishodia, Förster resonance energy transfer and molecular fluorescence near gain assisted refractory nitrides based plasmonic core-shell nanoparticle, *Plasmonics* **15**, 2081 (2020).
- [33] I. Issah, J. Pietila, T. Kujala, M. Koivurova, H. Caglayan, and M. Ornigotti, Epsilon-near-zero nanoparticles, *Physical Review A* **107**, 023501 (2023).
- [34] K. Murata, Y. Yasutake, K.-i. Nittoh, S. Fukatsu, and K. Miki, High-density g-centers, light-emitting point defects in silicon crystal, *AIP Advances* **1** (2011).
- [35] E. Rotem, J. M. Shainline, and J. M. Xu, Enhanced photoluminescence from nanopatterned carbon-rich silicon grown by solid-phase epitaxy, *Applied Physics Letters* **91** (2007).
- [36] M. W. Ngandeu Ngambou, P. Perrin, I. Balasa, A. Tira-

- nov, O. Brinza, F. Bénédic, J. Renaud, M. Reveillard, J. Silvent, P. Goldner, J. Achard, and A. Tallaire, Hot ion implantation to create dense NV center ensembles in diamond, *Applied Physics Letters* **124**, 134002 (2024).
- [37] Ansys/Lumerical, Fluorescence enhancement, <https://optics.ansys.com/hc/en-us/articles/360042161033-Fluorescence-enhancement>.
- [38] O. Yücel, S. Ateş, and A. Bek, Single-photon nanoantenna with in situ fabrication of plasmonic Ag nanoparticle at an hBN defect center, arXiv preprint arXiv:2003.13824 (2020).
- [39] Y.-C. Liu, B.-B. Li, and Y.-F. Xiao, Electromagnetically induced transparency in optical microcavities, *Nanophotonics* **6**, 789 (2017).
- [40] P. B. Johnson and R.-W. Christy, Optical constants of the noble metals, *Physical Review B* **6**, 4370 (1972).
- [41] E. D. Palik, *Handbook of optical constants of solids*, Vol. 3 (Academic press, 1998).
- [42] K. Shibata, H. Yuan, Y. Iwasa, and K. Hirakawa, Large modulation of zero-dimensional electronic states in quantum dots by electric-double-layer gating, *Nature Communications* **4**, 2664 (2013).
- [43] M. E. Tasgin, Many-particle entanglement criterion for superradiantlike states, *Physical Review Letters* **119**, 033601 (2017).
- [44] R. Alicki and M. Fannes, Entanglement boost for extractable work from ensembles of quantum batteries, *Physical Review E—Statistical, Nonlinear, and Soft Matter Physics* **87**, 042123 (2013).
- [45] D. Ferraro, M. Campisi, G. M. Andolina, V. Pellegrini, and M. Polini, High-power collective charging of a solid-state quantum battery, *Physical Review Letters* **120**, 117702 (2018).
- [46] D. Bluvstein, S. J. Evered, A. A. Geim, S. H. Li, H. Zhou, T. Manovitz, S. Ebadi, M. Cain, M. Kalinowski, D. Hangleiter, *et al.*, Logical quantum processor based on reconfigurable atom arrays, *Nature* **626**, 58 (2024).
- [47] P. Lodahl, A. Floris van Driel, I. S. Nikolaev, A. Irman, K. Overgaag, D. Vanmaekelbergh, and W. L. Vos, Controlling the dynamics of spontaneous emission from quantum dots by photonic crystals, *Nature* **430**, 654 (2004).
- [48] F. M. Stürner, A. Brenneis, T. Buck, J. Kassel, R. Rölver, T. Fuchs, A. Savitsky, D. Suter, J. Grimm, S. Hengsbach, *et al.*, Integrated and portable magnetometer based on nitrogen-vacancy ensembles in diamond, *Advanced Quantum Technologies* **4**, 2000111 (2021).
- [49] L. S. Madsen, F. Laudenbach, M. F. Askarani, F. Rortais, T. Vincent, J. F. Bulmer, F. M. Miatto, L. Neuhaus, L. G. Helt, M. J. Collins, *et al.*, Quantum computational advantage with a programmable photonic processor, *Nature* **606**, 75 (2022).